RESEARCH PAPER



A density-and-strain-based K-clustering approach to microstructural topology optimization

Tej Kumar¹ · Krishnan Suresh¹

Received: 27 October 2018 / Revised: 13 September 2019 / Accepted: 2 October 2019 / Published online: 21 November 2019 © Springer-Verlag GmbH Germany, part of Springer Nature 2019

Abstract

Microstructural topology optimization (MTO) is the simultaneous optimization of macroscale topology and microscale structure. MTO holds the promise of enhancing product-performance beyond what is possible today. Furthermore, with the advent of additive manufacturing, the resulting multiscale structures can be fabricated with relative ease. There are however two significant challenges associated with MTO: (1) high computational cost, and (2) potential loss of microstructural connectivity. In this paper, a novel density-and-strain-based K-means clustering method is proposed to reduce the computational cost of MTO. Further, a rotational degree of freedom is introduced to fully utilize the anisotropic nature of microstructures. Finally, the connectivity issue is addressed through auxiliary finite element fields. The proposed concepts are illustrated through several numerical examples applied to two-dimensional single-load problems.

Keywords Topology optimization · Microstructural optimization design · Clustering · Principal strain

1 Introduction

Topology optimization is a means of distributing material within a design domain, to optimize performance (Bendsøe and Sigmund 2004; Sigmund and Maute 2013). It is now a mature field with multitude of methods, including homogenization (Bendsøe and Kikuchi 1988; Hassani and Hinton 1998), Solid Isotropic Material with Penalization (SIMP) (Bendsøe 1989), level set approach (Sethian and Wiegmann 2000; Wang et al. 2003), topological sensitivity framework (Novotny et al. 2003; Deng and Suresh 2015; 2017), and evolutionary scheme (Xie and Steven 1993; Yang et al. 1999). As an example of topology optimization, Fig. 1a illustrates a compliance-optimized topology for a structural problem, computed via SIMP.

Responsible Editor: Ole Sigmund

☐ Tej Kumar tkumar3@wisc.edu

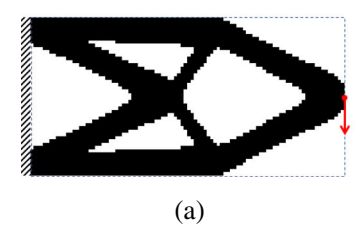
> Krishnan Suresh ksuresh@wisc.edu

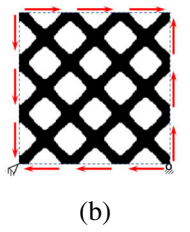
Department of Mechanical Engineering, University of Wisconsin-Madison, Madison, WI 53706, USA On the other hand, *microstructural design* is a technique for the distribution of material, at a smaller scale, to optimize material properties. Through microstructural design, one can customize various material behavior (Osanov and Guest 2016) including bulk/shear modulus (Huang et al. 2011), Poisson's ratio (Vogiatzis et al. 2017; Xie et al. 2014), thermal expansion (Sigmund and Torquato 1997), elasticity tensor (Sigmund 1994), and other extremal properties (Sigmund 2000). For example, Fig. 1b illustrates an optimal microstructure, once again computed via SIMP, for maximizing shear modulus.

Microstructural topology optimization (MTO) combines topology optimization and microstructural optimization, for simultaneously optimization of topology, at a macroscale, and microstructures at a smaller scale. For example, Fig. 1c illustrates an optimized MTO design. With the advancement in additive manufacturing (Gao et al. 2015; Liu et al. 2018b), such MTO designs can now be fabricated with relative ease. However, there are several challenges underlying MTO; the objective of this paper is to identify and address some of these challenges.

To understand these challenges, consider a typical MTO problem depicted in Fig. 2 where the objective is to construct an optimal topology and compute optimal microstructures over each macro finite element. This entails the following: Given an initial topology and an initial set







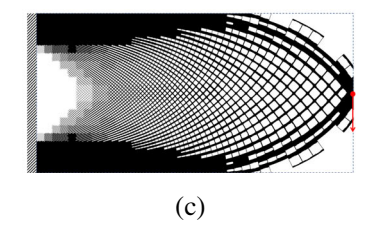


Fig. 1 Different design strategies. a Single scale design of short cantilever fixed on the left edge and loaded at the center of right edge. b 3×3 units of microstructures optimized for maximum shear stiffness. c MTO design using proposed method for same problem description as (a)

of (random) microstructures, (1) a microstructural analysis (numerical homogenization) is performed for each distinct microstructure, to extract the equivalent elasticity tensor (Rodrigues and Guedes 2002), (2) the elasticity tensors are then used to assemble a global stiffness matrix, (3) a macroscale analysis is carried out, (4) followed by sensitivity analysis, and (5) finally, the microdesign and macrodesign variables are updated, subject to various constraints. These five steps must be repeated numerous times, making MTO "very demanding" (Coelho et al. 2008) and computationally "quite massive" (Rodrigues and Guedes 2002). Efforts to reduce computational cost can often lead to sub-optimal designs. Further, ensuring topological connectivity between adjacent microstructures is also non-trivial. For example, in Fig. 2, the two microstructures with unit cells are not geometrically compatible when adjacent.

Various strategies have been proposed to address these challenges; these are reviewed in Section 2. In Section 3, we provide a generic MTO formulation. We discuss methods to alleviate the challenges in MTO by introducing cluster-based MTO design, which leads to a discussion on sensitivity analysis, and the proposed algorithm in Section 4. In Section 5, several numerical examples illustrate the proposed framework in context of two-dimensional single-load problems. We conclude the paper in Section 6, summarizing the current work and suggesting future work with open challenges.

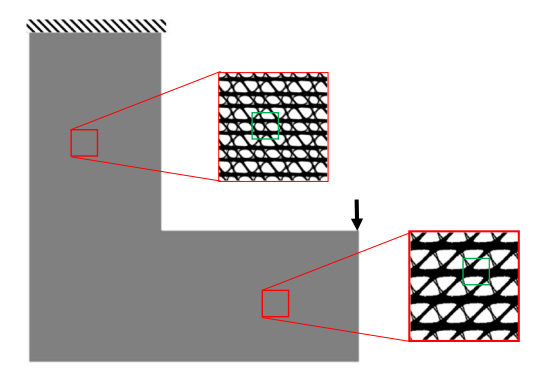


Fig. 2 Schematic of microstructural topology optimization



2 Literature review

As mentioned earlier, MTO poses two distinct challenges: (1) high computational cost, and (2) lack of connectivity between microstructures. Various strategies that have been proposed to resolve these challenges are discussed below.

2.1 Strategies to reduce computational cost

A simple strategy, specifically to reduce computational cost, is to constrain all microstructures to be identical. A single microstructure is then controlled by a set of microdesign variables, with no macrodesign variables (Huang et al. 2013). Due to its simplicity, the computational cost is significantly reduced, and connectivity can be guaranteed. However, the performance of the resulting structure is very poor, i.e., it is often much worse than a classic topology optimized design (Li et al. 2018).

An extension of the above strategy is to use a single microstructure, but also to include a density variable ρ_e over each macroelement (Liu et al. 2008; Deng et al. 2013; Yan et al. 2014). Then, the classic SIMP penalization function $f(\rho_e) = \rho_e^p$ can be used to control the presence or absence of each microstructure. The performance improves significantly with little or no additional computational cost. However, an artificial volume constraint must be imposed on the microstructures to avoid trivial solid/void designs. This leads to diminishing performance with decreasing microstructure's volume fraction (Sivapuram et al. 2016; Deng and Chen 2017). In other words, under this formulation, the very use of microstructures lowers performance!

A natural generalization is to allow a finite number of microstructures, rather than just one. For example, one can assume that macroelements with physical proximity share the same microstructural design, leading to the *grid-based clustering* (Sivapuram et al. 2016; Nakshatrala et al. 2013; Ferrer et al. 2017). Although the connectivity among neighboring microstructures in grid-based clustering can be handled efficiently (Du et al. 2018), the clustering is far from optimal (as will be demonstrated later on).

Alternately, variable-thickness design optimization (SIMP with p = 1) is first performed, and then macroelements with similar density ρ_e are assumed to have the same microstructural design (Li et al. 2018; Zhang et al. 2018; Liu et al. 2018a), leading to a density-based clustering. There are multiple methods for division of macroelements into clusters. For example, uniform density clustering which divides the range (0, 1] into R equal parts (Li et al. 2018), or uniform size clustering where macroelements sorted according to density are divided into equal sized clusters. Similarly, one can divide macroelements based on principal stress/strain directions (Xu and Cheng 2018). K-means clustering (Lloyd 1982) or k-clustering algorithm identifies already existing clusters in the given distribution of data (Liu et al. 2018a) (e.g., density or principal stress direction) and is likely to perform better than the uniform clustering methods.

In general, with *clustering*, performance improves, with a slight increase in computational cost (depending on the number of clusters).

2.2 Strategies to ensure connectivity

Connectivity has been addressed by several researchers: (1) if the microstructures are graded version of one parent microstructures, connectivity can be easily guaranteed (Wang et al. 2017a), (2) perturbation of coordinates may be used to achieve connected optimized structures (Liu et al. 2017; Zhu et al. 2019), (3) alternately, passive (non-design) microelements can be assigned to all microstructures for connectivity (Zhou and Li 2008; Deng and Chen 2017; Li et al. 2018), or, (4) a constraint on some connectivity measure can be introduced (Du et al. 2018), and (5) finally, if the microstructures are simple rotations of rectangular voids, it may be possible to ensure connectivity (Pantz and Trabelsi 2008; Groen and Sigmund 2018; Allaire et al. 2018). Use of parameterized rectangular voids renders these techniques computationally efficient. Alexandersen and Lazarov (2015) proposed an MTO technique without length-scale separation for better analysis and connectivity at an expense of high computational cost. A similar approach was earlier used by Zhang and Sun (2006) to study length-scale-related effect.

2.3 Alternate strategies

To solve both the computational complexity and the connectivity issue, *lattice structures* are used where the topology of the microstructure is fixed, but the lattice parameters are varied to achieve desired properties (Hassani and Hinton 1998; Cramer et al. 2016; Wang et al. 2017b).

However, the choice of the lattice topology is often arbitrary, and the performance is typically sub-optimal. Improved performance may be achievable by designing lattice structures on-the-fly (Wang et al. 2017a) or by better choice of lattice for the problem in hand, e.g., rectangular void aligned along principal direction (Groen and Sigmund 2018; Allaire et al. 2018).

Yet another strategy is the use of *rank-two laminates* (Francfort and Murat 1986; Avellaneda 1987; Jog et al. 1994) that are layers of solid interspersed with layers of striped solid and void. Since the effective properties of these laminates can be analytically computed, computational cost is reduced significantly. Their optimality for 2-dimensional compliance minimization problem has been demonstrated (Avellaneda 1987; Allaire et al. 2018). However, these laminates are not manufacturable.

The *free material optimization (FMO)* method has also been proposed (Bendsøe et al. 1994; Kočvara et al. 2008) where the objective is to first compute optimal elasticity tensors for each macroelement. Once this is complete, the next phase involves computing the microstructures that have the desired elasticity tensors (Schury et al. 2012). Realizability of the second phase is discussed in Milton and Cherkaev (1995). Unfortunately, the second phase can be computationally very demanding, and connectivity is not guaranteed.

2.4 Paper contributions

In this paper, we show that the performance can be improved significantly and consistently, by clustering elements based on the underlying strain tensor and the SIMP density, and adding a rotational degree of freedom. Connectivity is tackled using an additional finite element analysis. The main contributions of this paper are as follows:

- Describing various MTO methods, including the proposed one, as special cases of a single generic MTO formulation.
- 2. While the importance of SIMP density, and strain information for topology optimization, have been identified by Jog et al. (1994) and Bendsøe et al. (1994), we justify the importance of these two quantities for MTO clustering and provide a framework for exploiting them in MTO.
- Similarly, while the concept of rotational degree of freedom has been identified within the context of microstructural design (Bendsøe and Kikuchi 1988), we show that this concept can also be exploited for reducing the design space and for improved clustering.



3 Microstructural topology optimization design

Recall that MTO involves several steps including microstructural analysis, global stiffness matrix assembly, and macroanalysis. In this section, the mathematics behind these critical steps is described, together with typical design variables, objective, and constraints. Finally, a unified framework that captures popular MTO methods is also presented.

3.1 Design variables

In MTO, the domain is discretized into N macroelements, and each macroelement is further divided into M microelements as illustrated in Fig. 3. There are typically two sets of (SIMP) design variables (bounded by 0.001 and 1) corresponding to these elements, namely macrovariables and microvariables, resulting in a total of (N + NM) design variables. However, if a clustering strategy is used, several macroelements are mapped to a single microstructure, and they will share the same set of design variables. Consequently, with clustering, the total number of design variables will be reduced to (N + RM), where R is the number of distinct microstructures. Henceforth, in the presence of clustering, the mapping function from a macroelement nto a microstructure r will be denoted by r = g(n). The macrovariable will be denoted by ρ_n while the microvariable will be denoted by $\gamma_{r,m}$ corresponding to microelement m associated with a microstructure r.

3.2 Objective and constraints

In MTO, the typical objective is to minimize compliance $C = \mathbf{u}^T \mathbf{K} \mathbf{u}$

where K and u are global stiffness matrix and displacement vector, respectively. This is subjected to a global volume constraint:

$$v\sum_{n=1}^{N} \left(\rho_n \sum_{m=1}^{M} \gamma_{g(n),m} \right) \le V^* \tag{1}$$

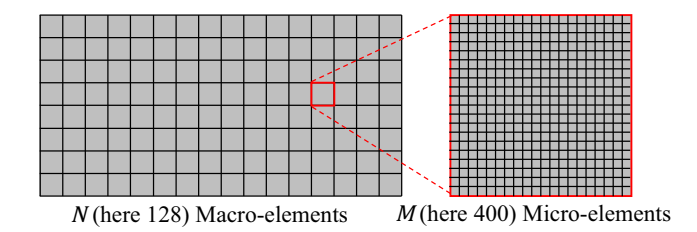
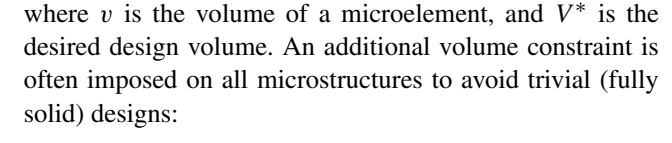


Fig. 3 Illustration of macroelements and microelements in a rectangular domain



$$v\sum_{m=1}^{M} \gamma_{r,m} \le v^*, \forall r \in \{1 \dots R\}$$
 (2)

There are variations to these generic constraints. For example, in the case of a single microstructure, i.e., R = 1, the volume constraint on microvariables is necessarily active. This simplifies Eq. 1 to $v^* \sum_{n=1}^{N} \rho_n \leq V^*$, making the global volume constraint independent of microdesign variables.

3.3 Microstructure analysis and homogenization

An important step in MTO is to compute the homogenized elasticity tensor for each distinct microstructure (Bendsøe and Kikuchi 1988). First the elasticity tensor of a microelement m is computed as $D_{r,m} = (\gamma_{r,m})^P D^0$ where D^0 is elasticity tensor of base material, and p is the SIMP penalization factor. The elasticity tensors are then exploited to assemble the microstructure stiffness matrix K_r . Three independent force vectors $f_r^{i=1,2,3}$ corresponding to three unit strains—two normal and one shear strain—are applied as illustrated in Fig. 4. By solving the corresponding three problems $K_r u_r^i = f_r^i$, the homogenized elasticity tensor D_r^H can be extracted (Liu et al. 2002). Note that these three problems must be solved for each of the R distinct microstructures.

3.4 Macroanalysis

Next, the homogenized elasticity tensor D_r^H is either directly used (Rodrigues and Guedes 2002; Nakshatrala et al. 2013), or scaled (Liu et al. 2008; Deng et al. 2013; Yan et al. 2014) via $\rho_n^P D_r^H$, to compute the stiffness matrix of each macroelement. In either case, these macroelement matrices are assembled into a global stiffness matrix K. Finally, the global problem Ku = f is solved, where f is the external force. The design variables are suitably updated

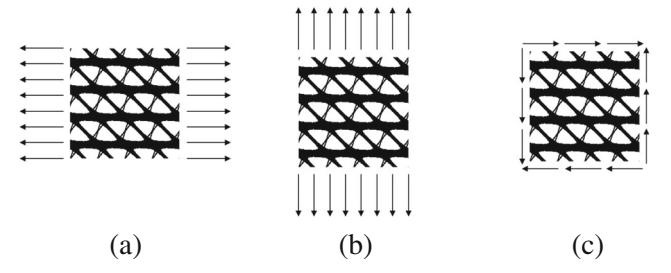


Fig. 4 Homogenization by analyzing microstructure thrice



(to be discussed later), and the process to repeated, until convergence is reached.

3.5 Generic formulation

Given the above definitions, almost all existing MTO (specifically, two scale) formulations can be captured via a generic MTO problem statement as follows.

minimize
$$u^{\mathsf{T}} K u$$
 (3a)

subject to
$$Ku = f$$
 (3b)

$$v \sum_{m=1}^{M} \gamma_{r,m} \le v^* \qquad \forall r \in \{1 \dots R\}$$
 (3c)

$$v\sum_{n=1}^{N} \left(\rho_n \sum_{m=1}^{M} \gamma_{g(n),m}\right) \le V^*$$
 (3d)

$$0.001 \le x_i \le 1 \qquad \forall i \tag{3e}$$

Various MTO formulations can be interpreted as special cases of the above formulation as in Table 1; references are provided for each formulation type. As one can observe, the design variables x, the constraints, and the definition of elasticity matrix for macroelements are different for each formulation. Performance with respect to classic topology optimization has also been compared for different methods, where performance less (greater) than 1 implies the MTO formulation performs worse (better) than classic topology optimization (performed using SIMP penalty p = 3). Two popular alternatives not included in the table are as follows: (1) variable-thickness design problem which has optimal performance, but violates Hashin-Shtrikman (1962) bounds and gives non-manufacturable design (Sigmund et al. 2016), and (2) the use of all design variables (NM) at one scale; this will provide optimized manufacturable design at a prohibitive computational cost. The above formulation can be easily modified for multiple load cased by adding equation for each load case in Eq. 3b and adding their contribution to Eq. 3a as weighted sum.

Later in the paper we will compare the proposed formulation (discussed next) against some of the formulations in Table 1.

4 Proposed method

In this section, we discuss the proposed method whose main highlights are as follows: (1) a simplified MTO formulation that eliminates macrodesign variables and microvolume constraints, (2) a "density-and-strain"-based clustering, (3) exploiting rotation variables to increase the design space, while enforcing connectivity.

4.1 Proposed clustering method

The proposed MTO formulation is a simplified version of the generic statement in Eq. 3:

$$\underset{\gamma_1, \gamma_2, \dots, \gamma_R}{\text{minimize}} \quad \boldsymbol{u}^\mathsf{T} \boldsymbol{K} \boldsymbol{u} \tag{4a}$$

subject to
$$Ku = f$$
 (4b)

$$v \sum_{n=1}^{N} \sum_{m=1}^{M} \gamma_{g(n),m} \le V^*$$
 (4c)

$$0.001 \le \gamma_{r,m} \le 1$$
 $1 \le r \le R$, $1 \le m \le M$ (4d)

Observe that, in the proposed formulation, there are no macroSIMP variables ρ_n . As a direct consequence, a single global volume constraint (see Eq. 4c) is sufficient; eliminating the microstructure volume constraint, which leads to better distribution of material. If $\kappa(r)$ denotes the cardinality of a microstructure r i.e. the number of

Table 1 Various MTO formulations as instances of the generic formulation

Problem type	x	Elasticity tensor	(3c)	(3d)	Performance
Classic topology optimization ¹	ρ	$\rho_n^p \mathbf{D}^0$	×	√	1
Single microstructure optimization ²	γ	$D^{\mathrm{H}}(\gamma)$	\checkmark	×	≪ 1
Single microstructure + macro-design ³	$ ho, \gamma$	$\rho_n^P \boldsymbol{D}^{\mathrm{H}}(\boldsymbol{\gamma})$	\checkmark	\checkmark	< 1
Unclustered microstructure optimization ⁴	$\boldsymbol{\gamma}_1, \boldsymbol{\gamma}_2, \dots, \boldsymbol{\gamma}_N$	$\boldsymbol{D}^{\mathrm{H}}(\boldsymbol{\gamma}_n)$	\checkmark	×	> 1
Clustered microstructures + macro-design ⁵	$\boldsymbol{\rho}, \boldsymbol{\gamma}_1, \boldsymbol{\gamma}_2, \dots, \boldsymbol{\gamma}_R$	$\rho_n^P \mathbf{D}^{\mathrm{H}}(\mathbf{\gamma}_r)$	\checkmark	\checkmark	< 1
Clustered microstructures + both constraints ⁶	$\boldsymbol{\rho}, \boldsymbol{\gamma}_1, \boldsymbol{\gamma}_2, \dots, \boldsymbol{\gamma}_R$	$\boldsymbol{D}^{\mathrm{H}}(\boldsymbol{\gamma}_r)$	\checkmark	\checkmark	≤ 1
Clustered microstructures ⁷	$\boldsymbol{\gamma}_1, \boldsymbol{\gamma}_2, \dots, \boldsymbol{\gamma}_R$	$\boldsymbol{D}^{\mathrm{H}}(\boldsymbol{\gamma}_r)$	\checkmark	×	§ 1

^{1,} Sigmund (2001); 2, Huang et al. (2013); 3, Liu et al. (2008), Deng et al. (2013), and Yan et al. (2014); 4, Rodrigues and Guedes (2002) and Nakshatrala et al. (2013); 5, Sivapuram et al. (2016); 6, Li et al. (2018) and Zhang et al. (2018); 7, Nakshatrala et al. (2013), Ferrer et al. (2017), and Liu et al. (2018a)



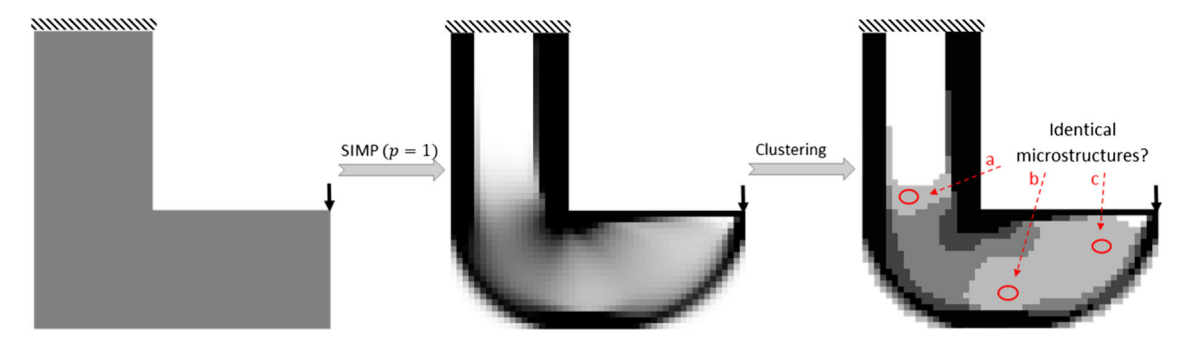


Fig. 5 Schematic of density-based clustering

macroelements associated with a microstructure r then the volume constraint can be expressed as follows:

$$v\sum_{r=1}^{R} \left(\kappa(r)\sum_{m=1}^{M} \gamma_{r,m}\right) \le V^* \tag{5}$$

rendering the mapping function g(n) dispensable for imposition of volume constraint.

4.2 Combined density-and-strain based clustering

In Section 2, we reviewed grid-based clustering and densitybased clustering. Here, we propose and justify a hypothesis that a "combined density-and-strain"-based clustering will lead to better performance. As a motivation, consider the pure density-based clustering illustrated in Fig. 5 where a variable thickness design optimization is first carried out; then the resulting density distribution is used to cluster macroelements. This method however disregards local strain conditions. For example, as illustrated in Fig. 5, the three macroelements "a, b, and c" with similar densities, but potentially different strain characteristics, are grouped into the same cluster. This, leads to sub-optimal microstructures, as illustrated later on through numerical experiments.

The proposed hypothesis (of strain-and-density-based clustering) is further supported by FMO (Bendsøe et al. 1994) where it is shown that the optimal elasticity

components at any location depends both on the local principal strains ε_I and ε_{II} , and the SIMP density ρ , i.e.,

$$D_{11} = \rho \frac{\varepsilon_I^2}{\varepsilon_I^2 + \varepsilon_{II}^2} \tag{6a}$$

$$D_{22} = \rho \frac{\varepsilon_{II}^2}{\varepsilon_I^2 + \varepsilon_{II}^2}$$

$$D_{12} = \rho \frac{\varepsilon_I \varepsilon_{II}}{\varepsilon_I^2 + \varepsilon_{II}^2}$$
(6b)
$$(6c)$$

$$D_{12} = \rho \frac{\varepsilon_I \varepsilon_{II}}{\varepsilon_I^2 + \varepsilon_{II}^2} \tag{6c}$$

Further, observe that it is sufficient to consider the strain ratio $\varepsilon_r^2 = \varepsilon_{II}^2/\varepsilon_I^2$, where $\varepsilon_{II}^2 \le \varepsilon_I^2$ to ensure $\varepsilon_r \in [0, 1]$. Thus, in this paper, we consider the two scalars $[\rho, \varepsilon_r^2]^T$ as a basis for clustering. In particular, we use Lloyd's Kmeans clustering algorithm (Lloyd 1982), together with Kmeans++ initialization (Arthur and Vassilvitskii 2007). The macroelements with density (obtained via variable thickness design optimization) close to 0, or close to 1, are constrained to two distinct clusters. The combined density-and-strainbased clustering is shown in Fig. 6. Note that the optimal periodic microstructure is not achievable when the principal strains are of opposite signs (Allaire and Aubry 1999). Therefore, the proposed clustering ignores differences in the optimized designs based on signs of principal strains (see Fig. 7 of Bendsøe and Sigmund (1999)). However, this leads to sub-optimal clustering. This clustering can also be performed on designs obtained via SIMP with penalization higher than 1 or via rank-2 laminate (Francfort and Murat

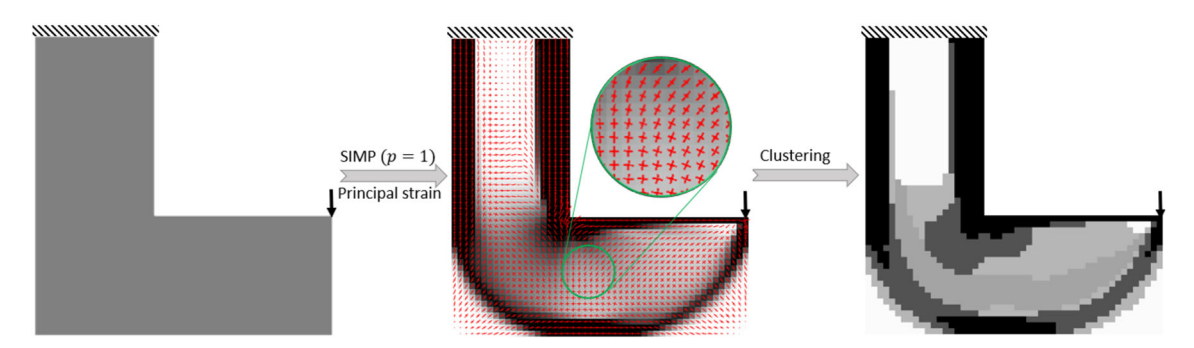


Fig. 6 Schematic of combined density-and-strain-based clustering



1986) design so as to not violate Hashin-Shtrikman bounds (1962).

4.3 Microstructure rotation

Observe that, by definition within a given cluster, macroelements have similar values for the density and principal-strain ratio. However, the principal strain direction can vary significantly within a cluster. Therefore, in order to map the macroelements within a cluster to a single parent microstructure, they must be rotated by an angle θ_n as determined by the principal direction (see Fig. 7).

Rotating microstructures along principal direction (Pedersen 1989) has two-fold advantage in clustering. The number of strain components is reduced from 3 to 2 (reducing the dimension of the problem), and better performance can be achieved with fewer clusters.

Further, due to this rotation, the elasticity tensor for each macroelement must also be transformed as follows: $D_n = Q(\theta_n)D^{\mathrm{H}}(\gamma_{g(n)})Q^{\mathrm{T}}(\theta_n)$ where rotation matrix $Q(\theta_n)$ is given by

$$\mathbf{Q}(\theta_n) = \begin{bmatrix} \cos^2(\theta_n) & \sin^2(\theta_n) & \sin(2\theta_n) \\ \sin^2(\theta_n) & \cos^2(\theta_n) & -\sin(2\theta_n) \\ -\sin(2\theta_n)/2 & \sin(2\theta_n)/2 & \cos(2\theta_n) \end{bmatrix}$$
(7)

This amounts to carrying out two matrix-matrix multiplications for each macroelement, during each step of the optimization process, followed by computing the corresponding

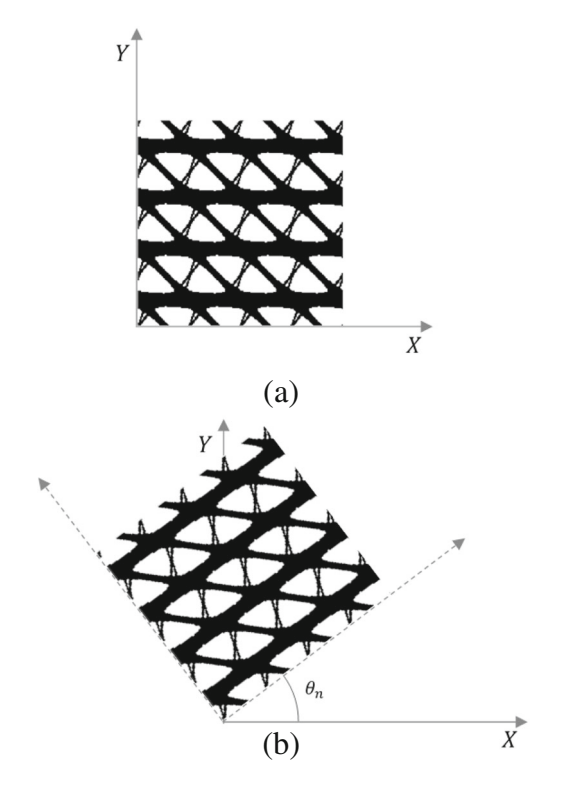


Fig. 7 a, b Rotation of microstructure by angle θ_n

element stiffness matrix. One can however significantly reduce the computational cost through elemental stiffness matrix K^{E} templates. Specifically, at the start of the optimization process, the following six templates are computed:

$$\hat{\mathbf{K}}_i = \mathbf{K}^{\mathrm{E}} \left(\hat{\mathbf{D}}_i \right) \qquad i = 1, \dots, 6 \tag{8}$$

where

$$\hat{\mathbf{D}}_{1} = \begin{bmatrix} 1 & 0 & 0 \\ 0 & 0 & 0 \\ 0 & 0 & 0 \end{bmatrix}, \quad \hat{\mathbf{D}}_{2} = \begin{bmatrix} 0 & 0 & 0 \\ 0 & 1 & 0 \\ 0 & 0 & 0 \end{bmatrix}, \quad \hat{\mathbf{D}}_{3} = \begin{bmatrix} 0 & 0 & 0 \\ 0 & 0 & 0 \\ 0 & 0 & 1 \end{bmatrix}, \\
\hat{\mathbf{D}}_{4} = \begin{bmatrix} 0 & 1 & 0 \\ 1 & 0 & 0 \\ 0 & 0 & 0 \end{bmatrix}, \quad \hat{\mathbf{D}}_{5} = \begin{bmatrix} 0 & 0 & 1 \\ 0 & 0 & 0 \\ 1 & 0 & 0 \end{bmatrix}, \quad \hat{\mathbf{D}}_{6} = \begin{bmatrix} 0 & 0 & 0 \\ 0 & 0 & 1 \\ 0 & 1 & 0 \end{bmatrix}$$

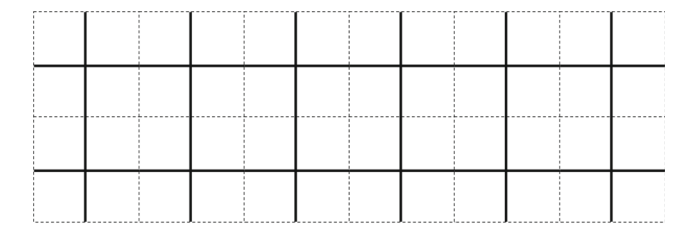
Then, during optimization, given a homogenized and transformed D matrix for each macroelement, the corresponding elemental stiffness matrix can be efficiently computed as follows:

$$\mathbf{K}^{E}(\mathbf{D}) = D_{11}\hat{\mathbf{K}}_{1} + D_{22}\hat{\mathbf{K}}_{2} + D_{33}\hat{\mathbf{K}}_{3} + D_{12}\hat{\mathbf{K}}_{4} + D_{13}\hat{\mathbf{K}}_{5} + D_{23}\hat{\mathbf{K}}_{6}$$
(9)

4.4 Connectivity of microstructures

Finally, we discuss the connectivity issue. Recall that all microstructures within a cluster map to the same parent microstructure, with possible rotation. If there is no rotation, then the connectivity within the cluster can be easily enforced (see Fig. 8a). However, in the presence of rotation, connectivity is typically lost; see Fig. 8b.

This can be addressed by morphing microstructures (Pantz and Trabelsi 2008; Allaire et al. 2018; Groen and



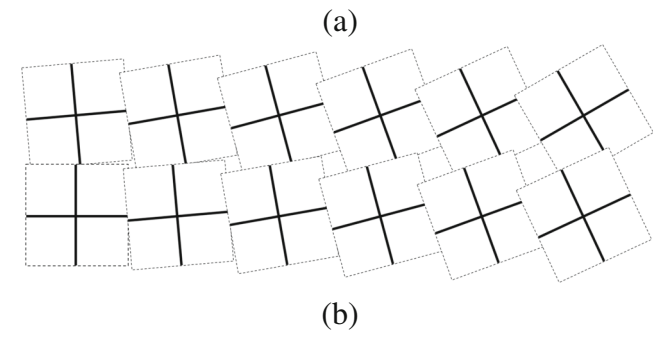


Fig. 8 a Arrangement of microstructures without rotation. b Desired rotations of microstructure



Sigmund 2018) using a continuously varying coordinate system oriented along principal strain directions. Observe that the strain directions are computed at the center of each macrocell and are therefore discontinuous, and must be smoothed. Moreover, the rotational symmetry of the direction field is handled using connected component labelling (Groen and Sigmund 2018).

Let the desired coordinate transformation be represented by $\tilde{x}(x, y)$ and $\tilde{y}(x, y)$ for every point (x, y) in the design domain. The gradients of this transformation are set equal to the principal strain directions n_1 and n_2 , where

$$n_1 = \begin{bmatrix} \cos(\theta) \\ \sin(\theta) \end{bmatrix}, \qquad n_2 = \begin{bmatrix} -\sin(\theta) \\ \cos(\theta) \end{bmatrix}$$

i.e.,

$$\nabla \tilde{x} = \mathbf{n}_1, \qquad \nabla \tilde{y} = \mathbf{n}_2 \tag{10}$$

In theory, these gradients only exist if curl of n_1 and n_2 vanishes everywhere in the domain Allaire et al. (2018), but this limitation can be disregarded in practice (see Fig. 13 and its explanation in Allaire et al. (2018)). Prior works by Allaire et al. (2018) and Groen and Sigmund (2018) consider a cosine function formulation that only applies to microstructures with rectangular voids. Here, we consider a variation of this concept that applies to any microstructure.

First, we impose the gradient constraint in a weak sense using a finite element formulation. In other words, the coordinate transformation fields \tilde{x} and \tilde{y} are described using standard finite element basis function N with unknown values \hat{x} and \hat{y} defined at the nodes. The gradient of the basis function is defined as $B = \nabla N$. This leads to a pair of linear systems:

$$\check{K}\hat{\hat{x}} = \check{F}_1, \qquad \check{K}\hat{\hat{y}} = \check{F}_2$$
(11)

where

$$\breve{K} = \int_{\Omega} \mathbf{B}^{\mathsf{T}} \mathbf{B} d\Omega
\breve{F}_{1} = \int_{\Omega} \mathbf{B}^{\mathsf{T}} \mathbf{n}_{1} d\Omega
\breve{F}_{2} = \int_{\Omega} \mathbf{B}^{\mathsf{T}} \mathbf{n}_{2} d\Omega$$

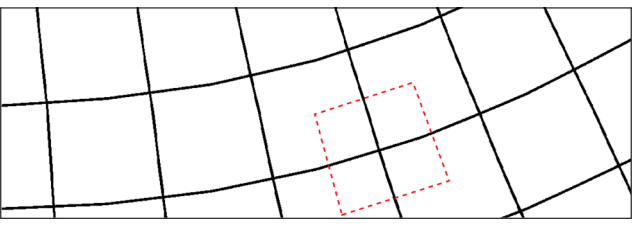
The two linear systems have the same stiffness matrix but different force vectors. The use of a finite element formulation used here (and also in Groen et al. (2019) applied to triangle wave function) simplifies the computation, and the resulting fields are free from oscillations as observed in finite difference formulation (Groen and Sigmund 2018).

Further, unlike the cosine (Allaire et al. 2018; Groen and Sigmund 2018) or triangle wave (Groen et al. 2019) formulation, in this paper, the coordinate transformation is

used directly to obtain a morphed set of microstructures. Every quad $(\tilde{x}_1, \tilde{y}_1, \tilde{x}_2, \tilde{y}_2)$ such that $(\tilde{x}_2 - \tilde{x}_1 = \Delta x)$, $(\tilde{y}_2 - \tilde{y}_1 = \Delta y)$ is mapped with a microstructure where $(\Delta x, \Delta y)$ is the size of a macroelement. This microstructure g(n) corresponds to the macroelement n with center closest to the center of the quad. These centers are computed in (x, y) as opposed to (\tilde{x}, \tilde{y}) used for quad identification. Figure 9 a demonstrates the morphed microstructures generated by using the above concept. The region marked in the figure corresponds to a quad which maps one microstructure.

The above formulation restricts isocontours of \bar{x} and \bar{y} to be equispaced, leading to their digression from desired path especially near regions of convergent principal strain directions. This is overcome by having a scalar associated with n_1 and n_2 which dictates the convergence or divergence of isocontours. We choose e^r as suggested by Allaire et al. (2018) and solve for r using an equation identical to Fig. 10a except that the right hand side becomes $[-\frac{\partial \theta}{\partial y}, \frac{\partial \theta}{\partial x}]^{\mathsf{T}}$ instead of n_1 or n_2 . As we do not eliminate singularities in strain field, which usually occurs in void region, we add weight w which is 0.01 in void regions (Groen and Sigmund 2018) and one everywhere else. Finite element formulation as described earlier is used first for the solution of $w\nabla r = w[-\frac{\partial\theta}{\partial y}, \frac{\partial\theta}{\partial x}]^{\mathsf{T}}$ followed by the solution of modified Eq. 10 i.e. $w\nabla \bar{x} = we^r \mathbf{n}_1$ and $w\nabla \bar{y} = we^r \mathbf{n}_2$. Figure 9 b illustrates the morphed microstructures generated by using the modified equations.

As the isocontour spacing is no longer uniform, they must be properly scaled. Based on our experience, a scaling factor of $2\Delta x/\overline{||\nabla \bar{x}||}$ for \bar{x} and $2\Delta y/\overline{||\nabla \bar{y}||}$ for \bar{y} is suggested. This factor is problem dependent and needs to be chosen properly to avoid too coarse or too dense quads. Note that even for the same parent microstructure, the size of the



(a) Without scalar parameter r.

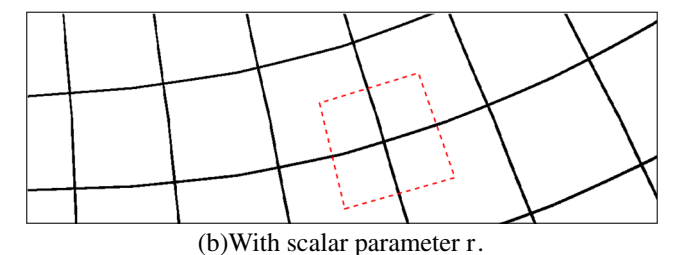


Fig. 9 a, b Morphed microstructures using the continuously varying coordinate system. Highlighted region is mapping of one quad



quad determines the feature size which varies significantly throughout the domain. Note the variation in the size of microstructures from left (compressed) to right (expanded) in Fig. 9b as compared with Fig. 9a.

After generating the design, a full-scale analysis is performed as a verification step. However, low-volume fraction regions with compressed microstructures may exhibit disconnectedness (see Fig.10a) which will lead to a singular stiffness matrix. Therefore, a $10\times$ finer discretization (in both direction) of the design domain is used to arrive at final design (as shown in Fig. 10b), which is then agglomerated in a mesh with (NM) elements (as shown in Fig. 10c) to enable full-scale analysis. In the full-scale analysis, elements are penalized with a penalty parameter of 3 to prevent performance over-estimation (Hashin and Shtrikman 1962). This two-step approach obviates post-processing of disconnected features.

As a final comment on connectivity, observe that microstructures with their axes oriented along principal directions, when optimized, give rise to Vigdergauz-like structures (Vigdergauz 1989; 1994; Bendsøe and Sigmund 1999) illustrated in Fig. 11. In other words, if a microstructure exists (with non-zero density and principal stress ratio), the boundary of the microstructure is always solid. Thus, we can force the boundary of such microstructures to be a non-design region, as illustrated in Fig. 12. This ensures connectivity between clusters as well. There may be regions not fully solid or void with one principal stress vanishing, then the non-design regions of a microstructure ensure connectivity at the cost of rendering it non-optimal.

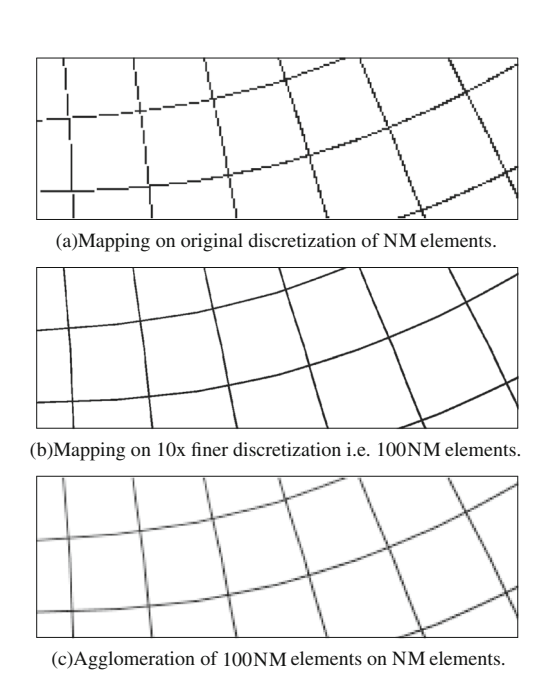


Fig. 10 Agglomeration to ensure connectivity for full-scale analysis

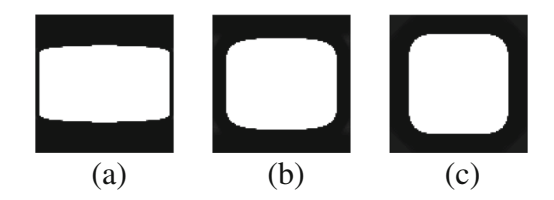


Fig. 11 Microstructure design for volume fraction of 0.5 and principal stress ratio $\mathbf{a} \frac{\sigma_{II}}{\sigma_I} = 0.1$, $\mathbf{b} \frac{\sigma_{II}}{\sigma_I} = 0.5$, and $\mathbf{c} \frac{\sigma_{II}}{\sigma_I} = 1$

4.5 Sensitivity analysis and design update

We now develop the sensitivity equations; the sensitivity of compliance C with respect to the microdesign variable $\gamma_{r,m}$ is given by:

$$\frac{\partial C}{\partial \gamma_{r,m}} = \boldsymbol{u}^{\mathsf{T}} \frac{\partial \boldsymbol{K}}{\partial \gamma_{r,m}} \boldsymbol{u} + 2\boldsymbol{u}^{\mathsf{T}} \boldsymbol{K} \frac{\partial \boldsymbol{u}}{\partial \gamma_{r,m}}$$
(12)

where the symmetry of global stiffness matrix K has been exploited. We will assume that the load is design independent. Therefore, from the governing equation Ku = f, we have

$$K\frac{\partial \mathbf{u}}{\partial \gamma_{r,m}} = -\frac{\partial K}{\partial \gamma_{r,m}}\mathbf{u}$$

Substituting this in Eq. 12 leads to

$$\frac{\partial C}{\partial \gamma_{r,m}} = -\boldsymbol{u}^{\mathsf{T}} \frac{\partial \boldsymbol{K}}{\partial \gamma_{r,m}} \boldsymbol{u} \tag{13}$$

One can express this as a sum over all the macroelements

$$\frac{\partial C}{\partial \gamma_{r,m}} = -\sum_{n=1}^{N} \mathbf{u}_{n}^{\mathsf{T}} \frac{\partial K_{n}^{E}}{\partial \gamma_{r,m}} \mathbf{u}_{n} \tag{14}$$

Exploiting Eq. 9, the derivative of an elemental stiffness matrix can be expressed as

$$\frac{\partial \mathbf{K}_{n}^{E}}{\partial \gamma_{r,m}} = \hat{\mathbf{K}}_{1} \left(\frac{\partial D_{n}}{\partial \gamma_{r,m}} \right)_{11} + \hat{\mathbf{K}}_{2} \left(\frac{\partial D_{n}}{\partial \gamma_{r,m}} \right)_{22}
+ \hat{\mathbf{K}}_{3} \left(\frac{\partial D_{n}}{\partial \gamma_{r,m}} \right)_{33} + \hat{\mathbf{K}}_{4} \left(\frac{\partial D_{n}}{\partial \gamma_{r,m}} \right)_{12}
+ \hat{\mathbf{K}}_{5} \left(\frac{\partial D_{n}}{\partial \gamma_{r,m}} \right)_{13} + \hat{\mathbf{K}}_{6} \left(\frac{\partial D_{n}}{\partial \gamma_{r,m}} \right)_{23}$$
(15)

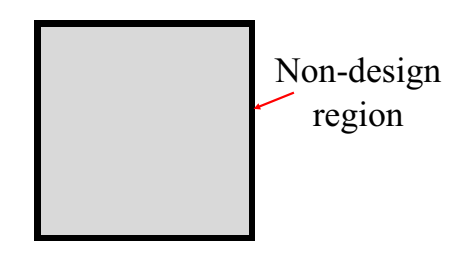


Fig. 12 Proposed non-design elements (shown in dark color) for ensuring connectivity



where $\boldsymbol{D}_n = \boldsymbol{Q}(\theta_n) \boldsymbol{D}_r^{\mathrm{H}}(\boldsymbol{\gamma}_r) \boldsymbol{Q}^{\mathsf{T}}(\theta_n)$. Finally, due to the

$$\frac{\partial \boldsymbol{D}_{n}}{\partial \gamma_{r,m}} = \begin{cases} \boldsymbol{Q}(\theta_{n}) \frac{\partial \boldsymbol{D}_{r}^{H}}{\partial \gamma_{r,m}} \boldsymbol{Q}^{\mathsf{T}}(\theta_{n}), & \text{if } r = g(n) \\ \boldsymbol{0}, & \text{otherwise} \end{cases}$$
(16)

Sensitivity of homogenized elasticity tensor is derived using the periodicity of microstructure (Liu et al. 2002). The sensitivity of the volume constraint in Eq. 5 is given by $v\kappa(r)$.

To avoid checker-boarding (Jog et al. 1994), the following sensitivity filter (Sigmund 2007) is used

$$\frac{\widetilde{\partial C}}{\partial \gamma_{r,m}} = \frac{1}{\gamma_{r,m}} \sum_{i \in \Theta_m} W_{mi} \gamma_{r,i} \frac{\partial C}{\partial \gamma_{r,i}}$$
(17)

where W_{mi} is cone type signed distance function, and Θ_m is the set of neighboring microelements. Note that the filters used for MTO must account for periodicity of microstructures (Xu and Cheng 2018). Further, in order to obtain solid/void designs, the filter radius is decreased from 4 to 1 (relative to micro-element width), in steps of 0.5, each time the relative change in compliance drops below 1×10^{-4} in two consecutive iteration; this is an accepted practice in SIMP to arrive at solid/void designs (Sigmund 2007).

The ratio of sensitivities of objective and volume constraint is contained in the term

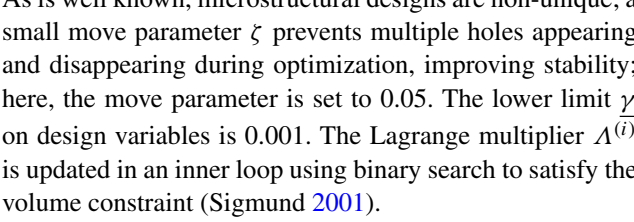
$$B_{r,m}^{(i)} = -\left(\left(\frac{\widetilde{\partial C}}{\partial \gamma_{r,m}}\right)^{(i)} / \Lambda^{(i)} v \kappa(r)\right)^{\eta}$$
(18)

where $\Lambda^{(i)}$ is the Lagrange multiplier corresponding to the volume constraint, η is the damping parameter set to 0.5, and i is current iteration index. The design update is carried out using the well-known optimality criteria method (Sigmund 2001) utilizing Eq. 18

$$\gamma_{r,m}^{(i+1)} = \begin{cases} \max\left(\gamma_{r,m}^{(i)} - \zeta, \underline{\gamma}\right) & \text{if } \gamma_n^{(i)} B_{r,m}^{(i)} \le \max\left(\gamma_{r,m}^{(i)} - \zeta, \underline{\gamma}\right) \\ \min\left(\gamma_{r,m}^{(i)} + \zeta, 1\right) & \text{if } \min\left(\gamma_{r,m}^{(i)} + \zeta, 1\right) \le \gamma_{r,m}^{(i)} B_{r,m}^{(i)} \\ \gamma_{r,m}^{(i)} B_{r,m}^{(i)} & \text{otherwise} \end{cases}$$

$$(19)$$

As is well known, microstructural designs are non-unique; a small move parameter ζ prevents multiple holes appearing and disappearing during optimization, improving stability; here, the move parameter is set to 0.05. The lower limit γ on design variables is 0.001. The Lagrange multiplier $\Lambda^{(i)}$ is updated in an inner loop using binary search to satisfy the





4.6 Algorithm

A flowchart depicting the proposed algorithm is illustrated in Fig. 13. The algorithm can be divided into three distinct phases, and these are described below.

The first phase starts with initialization and discretization of design domain with macroelements and microelements. Then, variable-thickness design optimization is performed over the macroelements. This is followed by computation of principal strain ratio and principal directions. The SIMP density and the principal strain ratio are exploited to perform K-clustering. This divides the macroelements into R clusters. The microdensity variables for each of the R clusters are initialized as in Fig. 14, where the difference between the two regions is 0.2, while the mean density of the microstructures is matched with the SIMP density. This ensures that the sensitivity values do not vanish everywhere.

In the second phase, homogenization carried out for each of the R microstructures, followed by macroanalysis. The sensitivity is computed and filtered using Eq. 17; the design variables are updated as described earlier. This process is repeated until either the change in microvariables is small (here, 0.005), or the relative change in objective is small (here, 5×10^{-6}).

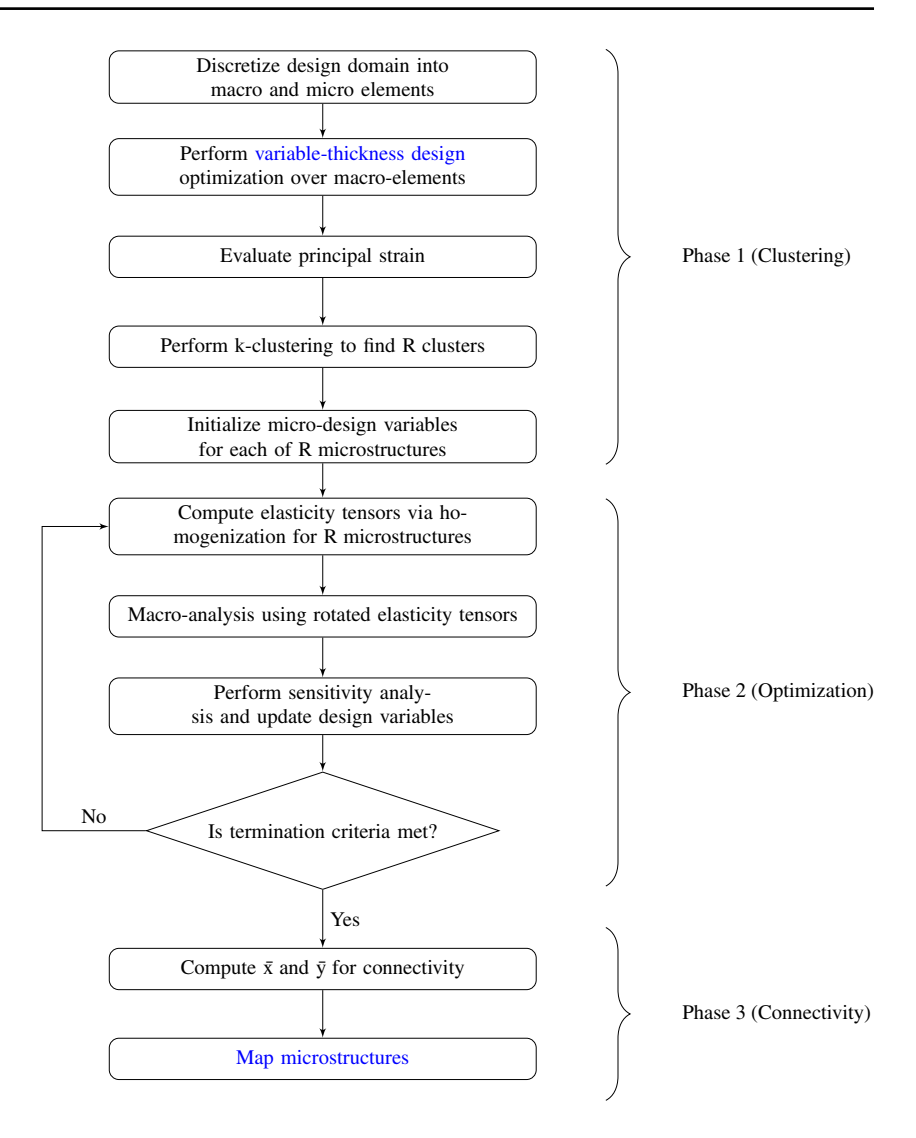
When the optimization terminates, the algorithm enters the third phase where the microstructures are morphed and mapped on a ten times finer mesh to ensure connectivity. Then, a final analysis of the mapped design is performed by agglomeration, as described earlier. In the following examples, the compliance values obtained using full-scale analysis are reported in parenthesis along with the values obtained using homogenization approach.

5 Numerical examples

5.1 Microstructural design validation

We consider an example from Zhang and Sun (2006) where the rectangular design domain, illustrated in Fig. 15, is fixed on the left edge and a uniform shear load is applied on the right edge. The domain is discretized into 16×10 (macro) elements which are then clustered into 10 different horizontal layers. The top and bottom layers are made solid as in Zhang and Sun (2006), and the remaining layers have a distinct microstructure, leading to a total of 8 different microstructures (using grid-based clustering to be consistent with the published result in Zhang and Sun (2006)). Each macroelement is divided into 1600 microelements. The Young's modulus is 1000, and Poisson's ratio is 0.3. No connectivity is enforced among different microstructures. The compliance is minimized for an overall volume fraction of 0.6.

Fig. 13 Flowchart of proposed MTO algorithm



The design obtained by Zhang and Sun (2006) is illustrated in Fig. 16a, while the design obtained via the proposed method is illustrated in Fig. 16b. The compliance for the design in Zhang and Sun (2006) was reported as 172171.8, while the compliance of the proposed design is 145583. For comparison, a full-scale analysis was performed on the final design with 0.25 million elements,

resulting in a compliance of 147806. Thus, in this case, homogenization leads to an error of less than 2%. The difference can be attributed to the filtering method; the method used here leads to a distinct solid/void design, resulting in a lower compliance value. No finer mesh mapping is required because of the absence of any morphing in this example.

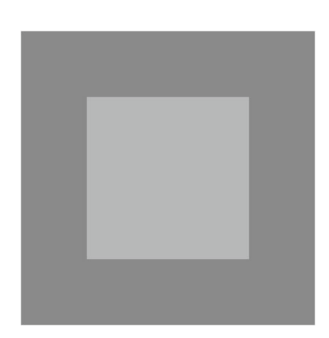


Fig. 14 Microstructure initialization

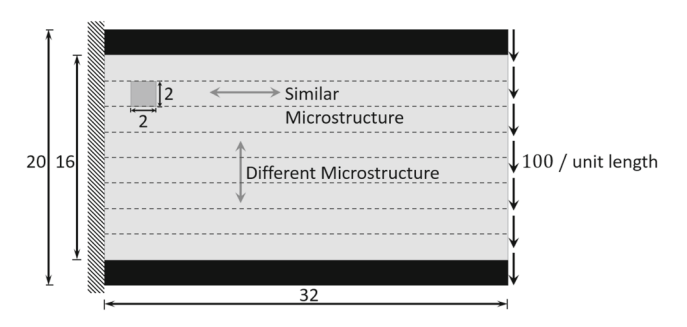


Fig. 15 Design domain and microstructure from Zhang and Sun (2006)



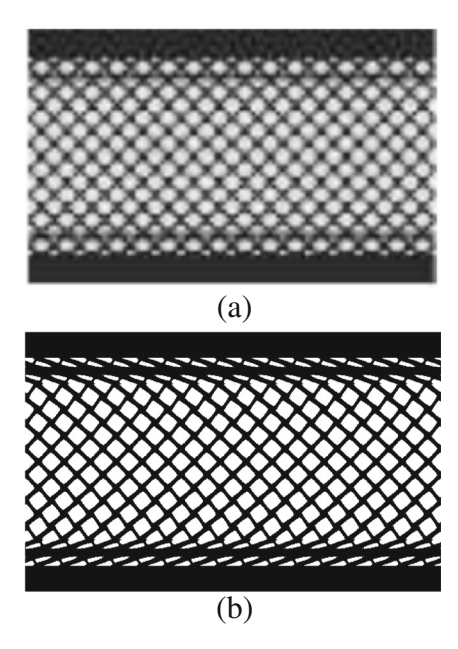


Fig. 16 Design comparison: **a** as illustrated in Zhang and Sun (2006), and **b** obtained via proposed method

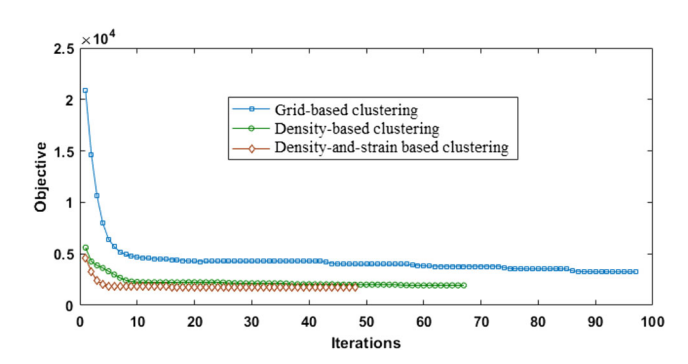


Fig. 18 Convergence history for the three types of clustering

5.2 Comparison of clustering methods

We will now compare the proposed density-and-strain-based clustering against grid-based clustering and density-based clustering. Observe that the clustering method only affects phase 1 of the algorithm. The design domain is an L-bracket (see Fig. 17a), discretized into 1600 macroelements where each macroelement is further divided into 1600

Fig. 17 L-bracket to perform cluster-based MTO. a Design domain; grid-based clustering: b clusters and c design; density-based clustering: d density from variable-thickness design optimization, e clusters, and f design; combined density-and-strain-based clustering: g density from variable-thickness design optimization and principal strain, h clusters, and i design

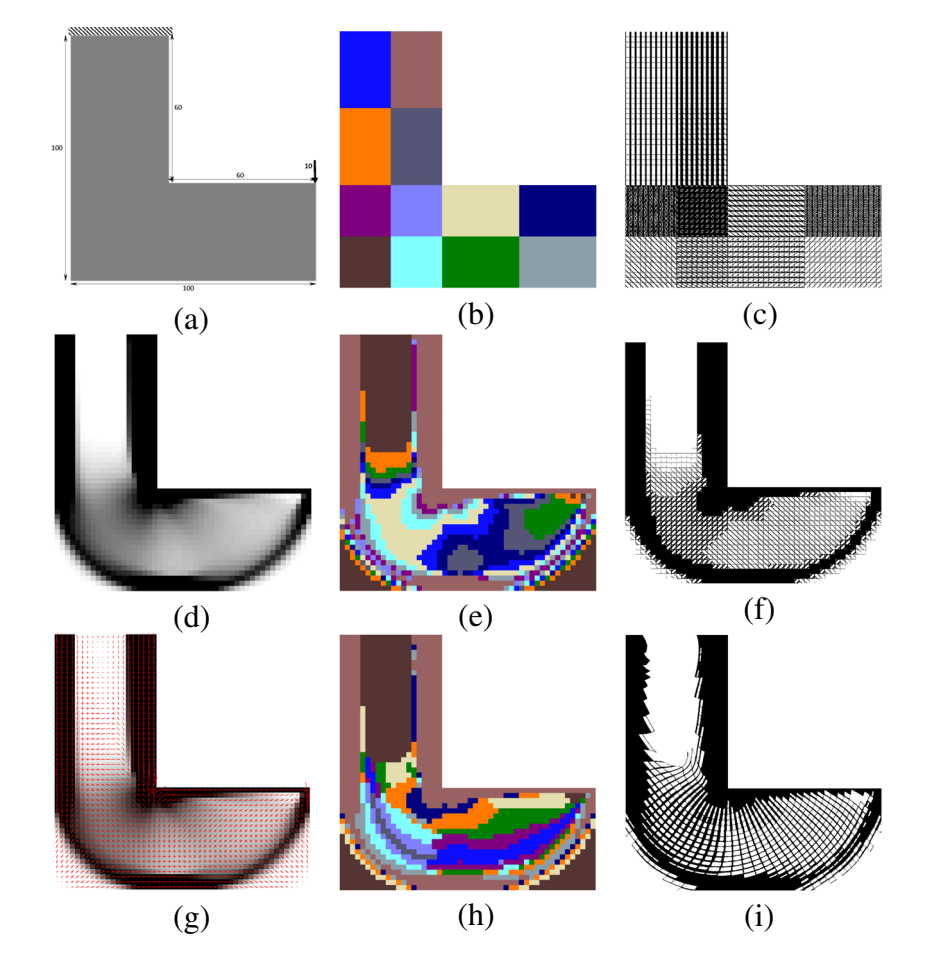




Table 2 L-bracket: final objective and computation time; the quantity within parenthesis is obtained by a full-scale analysis of the final design, without homogenization

Clustering type	Final objective	Iterations	Computation time (s)	Avg. Time per iteration (s)
Grid	3096.4 (3238.7)	115	592	6.1
Density	1936.4 (2086.50)	67	424	6.3
Density-and-strain	1717.3 (2056.02)	48	586	12.2

microelements. The Young's modulus is 10 and Poisson's ratio is 0.3; the number of clusters R is chosen to be 12 and desired global volume fraction is 0.5.

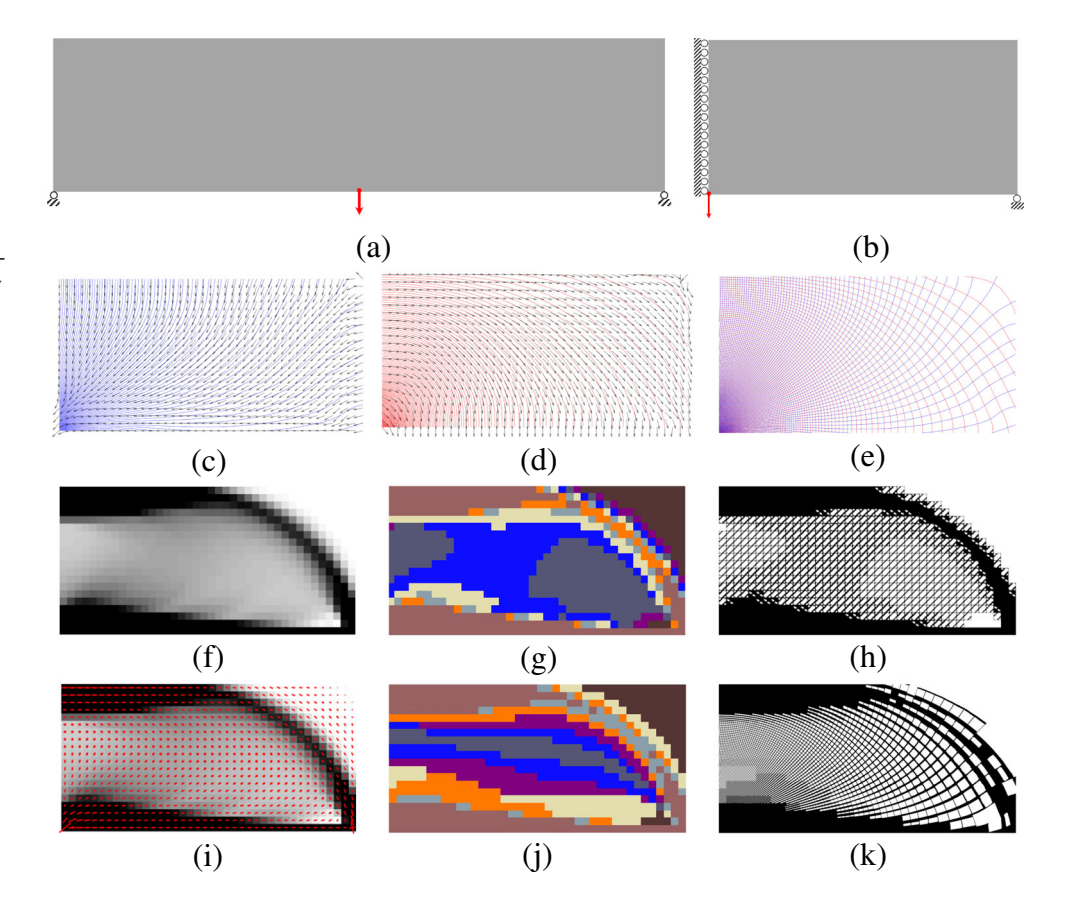
For grid-based clustering, adapting from Sivapuram et al. (2016), the domain is divided into 12 regions as illustrated in Fig. 17b. The optimized design is given in Fig. 17c. For density-based clustering, first, variable-thickness design optimization is carried out (see Fig. 17d). This is used to form clusters as illustrated in Fig. 17e, resulting in the design shown in Fig. 17f. Finally, using the proposed density-and-strain-based method, the clusters are formed as illustrated in Fig. 17h, while Fig. 17 i illustrates the final design.

The convergence plots for the three cases are illustrated in Fig. 18. The staircase shape obtained in convergence history

is due to the change in sensitivity filter radius. The compliances and computational costs are summarized in Table 2. As expected, the compliance from the proposed method is better than the other two using homogenization with no significant increase in computational cost. The mesh for full-scale analysis consists of 2.56 million elements.

For further validation, consider a bridge problem shown in Fig. 19a. The Young's modulus is 2.1×10^5 and Poisson's ratio 0.3. The design domain is shown in Fig. 19b having a point force of 1000, whereas the contours of \tilde{x} and \tilde{y} along with the principal directions are shown in Fig. 19c to e. The optimization results are shown for density (see Fig. 19h) and density-and-strain-based (see Fig. 19k) clustering methods with objective values 418.08 (490.53) and 342.26 (466.95), respectively. The improved compliance values in these

Fig. 19 Bridge problem: **a** problem domain, **b** design domain; Auxiliary fields: **c** direction n_1 and \bar{x} , **d** direction n_2 and \bar{y} , **e** \bar{x} and \bar{y} ; densitybased clustering: **f** density from variable-thickness design optimization, **g** clusters, and **h** design; combined density-andstrain-based clustering: **i** density from variable-thickness design optimization and principal strain, **j** clusters, and **k**) design





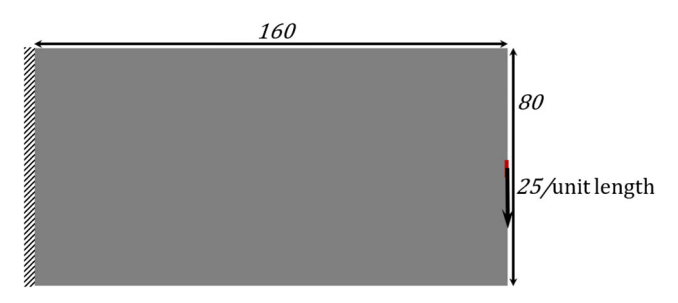


Fig. 20 Short cantilever fixed on the left edge and loaded on the center of right edge. Length of line of load = 8

two examples validate the superiority of density-and-strain-based clustering over density-based clustering. The full scale analysis is performed on a 800×1600 mesh.

5.3 Effect of number of clusters and comparison against SIMP design

Here, we compare and show the benefit of proposed method, against variable thickness and SIMP (p=3) designs; we will also study the effect of the number of clusters. As an example, we consider a short cantilever beam with mid-edge load on the right edge illustrated in Fig. 20. The domain is discretized into 800 macroelements, where each macroelement is subdivided into 1600 microelements. The

Young's modulus is 2.1×10^5 , Poisson's ratio is 0.3, and desired volume fraction is 0.5.

The designs from variable-thickness and SIMP (p =3) optimization performed on macroelement discretization are illustrated in Fig. 21 a and b, respectively. Designs obtained for various choices of number of clusters using the proposed method are illustrated in the Fig. 21c to f. Table 3 summarizes the results for different cases. An increase in compliance in full-scale analysis (performed on a 800×1600 mesh) is expected since we are distorting the generated microstructures. However, the large disparity in the two numbers may be attributed to a lot of gray elements and imperfect morphing, which requires further Notice that the increase in number of clusters enhances the performance, but it does not approach the variable thickness design or surpass SIMP (p = 3)design in full-scale analysis. This is attributed to clustering performed only once at the start of the optimization process. Dynamic clustering may lead to improved performance and will be pursued in future. Further, the poor performance for 3 cluster case is due to the assignment of all the macroelements to one cluster except for those assigned to the two constrained (with variable thickness design density close to 0 or 1) clusters. As expected, the average time per iteration increases with increase in the number of clusters. In case of no-clustering, i.e., clusters equal to number of macroelements (800 in this case), the average time per iteration blows up to 22 min.

Fig. 21 a Variable-thickness design. **b** SIMP (p = 3) design. Designs with different number of clusters: **c** R = 3, **d** R = 5, **e** R = 10, and **f** R = 15

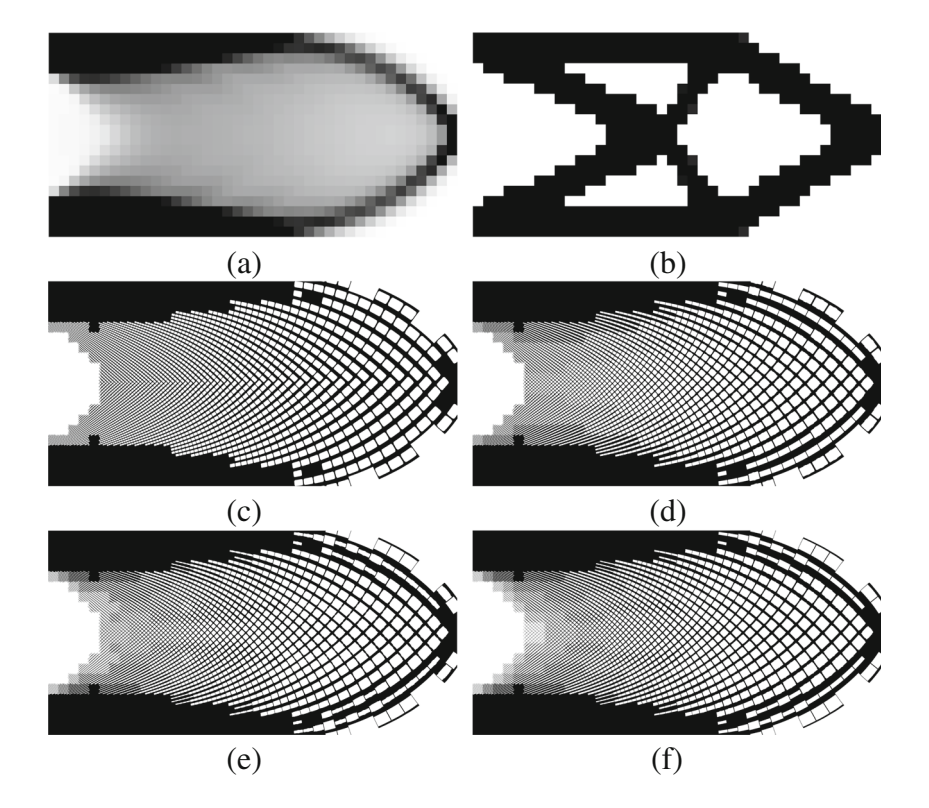




Table 3 Compliance for short cantilever beam with mid-edge load

Figure	Туре	Number of clusters	Compliance	Iterations	Avg. time per iteration (s)
21a	Variable thickness design	-	10.335	82	0.03
21b	SIMP $(p = 3)$ design	_	11.86	51	0.06
21c	Clustered design	3	12.07 (14.10)	49	5.57
21d	Clustered design	5	11.49 (13.0)	49	5.73
21e	Clustered design	10	11.38 (12.84)	58	5.82
21f	Clustered design	15	11.34 (12.74)	50	5.96

6 Conclusion

In this paper, a generic MTO formulation is provided which encompasses most of the MTO problems in published literature. The challenges associated with MTO such as large computational cost and loss of connectivity due to the presence of microstructures are tackled in the proposed method. This comprises three distinct phases: clustering, optimizatio, and connectivity. In the first phase, a novel combined density-and-strain-based clustering method is proposed to divide macroelements into a pre-defined number of clusters. During the next phase, rotated microstructures are optimized for minimizing the compliance. These rotations are based on principal directions. In the final phase, connectivity of rotated microstructures is ensured by solving a pair of linear system to define a transformation field. This field is used to project computed microstructures into the design domain.

The proposed clustering method is demonstrated to perform well for small number of clusters. Its superiority as compared with other clustering methods has been demonstrated. K-clustering is used to tackle clustering of two-dimensional parameter involving density ρ and principal strain ratio $(\varepsilon_{II}/\varepsilon_I)^2$. The anisotropic nature of microstructures is effectively utilized by adding the rotational degree of freedom. A simpler method of handling microstructure connectivity for rotated microstructures is proposed as compared with existing methods. The effectiveness of proposed method is also manifested by fewer number of iterations required for convergence.

There are certain aspects of the work which needs to be pursued in future. Starting with a dynamic clustering scheme to redistribute clusters according to evolving design and strain field, which is likely to improve the performance further. A smooth variation is not obtained in the presence of singularity in strain directions as shown by Allaire et al. (2018) and therefore, the auxiliary coordinate system distorts in the neighborhood of singularity. An approach to identify and handle these singularities will be dealt in future along with extending this work to 3D and for objectives other than compliance. Since density-and-strain-based clustering and principal-strain-based rotation may

not be applicable to non-compliance problems, alternate strategies need to be explored.

7 Replication of results

The MATLAB code and data files required to replicate results presented here are available at http://www.ersl.wisc.edu/software/MTO_Code.zip.

Funding information The authors would like to thank the support of the National Science Foundation through grant 1561899. Prof. Krishnan is a consulting Chief Scientific Officer of SciArt, Corp, which has licensed the Pareto technology, developed in Prof. Suresh's lab, through Wisconsin Alumni Research Foundation.

Compliance with ethical standards

Conflict of interests The authors declare that they have no conflict of interest.

References

Alexandersen J, Lazarov BS (2015) Topology optimisation of manufacturable microstructural details without length scale separation using a spectral coarse basis preconditioner. Comput Meth Appl Mech Eng 290(290):156–182. arXiv:1411.3923

Allaire G, Aubry S (1999) On optimal microstructures for a plane shape optimization problem. Structural Optimization 17(2):86–94 Allaire G, Geoffroy-Donders P, Pantz O (2018) Topology optimization of modulated and oriented periodic microstructures by the homogenization method. Computers and Mathematics with Applications

Arthur D, Vassilvitskii S (2007) K-means++: the advantages of careful seeding. Proceedings of the eighteenth annual ACM-SIAM symposium on Discrete algorithms, pp 1027–1025. arXiv:1212.1121

Avellaneda M (1987) Optimal bounds and microgeometries for elastic two-phase composites. Siam J Appl Math 47(6):1216–1228

Bendsøe MP (1989) Optimal shape design as a material distribution problem. Structural Optimization 1(4):193–202

Bendsøe MP, Kikuchi N (1988) Generating optimal topologies in structural design using a homogenization method. Comput Methods Appl Mech Eng 71(2):197–224

Bendsøe MP, Sigmund O (1999) Material interpolation schemes in topology optimization. Arch Appl Mech 69(9-10):635–654



- Bendsøe MP, Sigmund O (2004) Topology optimization. Springer, Berlin
- Bendsøe MP, Guedes JM, Haber RB, Pedersen P, Taylor JE (1994) An analytical model to predict optimal material properties in the context of optimal structural design. J Appl Mech 61(4):930
- Coelho PG, Fernandes PR, Guedes JM, Rodrigues HC (2008) A hierarchical model for concurrent material and topology optimisation of three-dimensional structures. Struct Multidiscip Opt 35(2):107–115
- Cramer AD, Challis VJ, Roberts AP (2016) Microstructure interpolation for macroscopic design. Struct Multidiscip Optim 53(3):489–500
- Deng J, Chen W (2017) Concurrent topology optimization of multiscale structures with multiple porous materials under random field loading uncertainty. Struct Multidiscip Optim 56(1):1–19
- Deng S, Suresh K (2015) Multi-constrained topology optimization via the topological sensitivity. Struct Multidiscip Optim 51(5):987–1001
- Deng S, Suresh K (2017) Stress constrained thermo-elastic topology optimization with varying temperature fields via augmented topological sensitivity based level-set. Structural and Multidisciplinary Optimization 56(6):1413–1427
- Deng J, Yan J, Cheng G (2013) Multi-objective concurrent topology optimization of thermoelastic structures composed of homogeneous porous material. Struct Multidiscip Optim 47(4):583–597
- Du Z, Zhou X, Picelli R, Kim HA (2018) Connecting microstructures for multiscale topology optimization with connectivity index constraints. J Mech Des 140(11):111417
- Ferrer A, Cante JC, Hernández JA, Oliver J (2017) Two-scale topology optimization in computational material design: an integrated approach. Int J Numer Methods Eng 114:232–254
- Francfort GA, Murat F (1986) Homogenization and optimal bounds in linear elasticity. Arch Ration Mech Anal 94(4):307–334
- Gao W, Zhang Y, Ramanujan D, Ramani K, Chen Y, Williams CB, Wang CCL, Shin YC, Zhang S, Zavattieri PD (2015) The status, challenges, and future of additive manufacturing in engineering. CAD Computer Aided Design 69:65–89
- Groen JP, Sigmund O (2018) Homogenization-based topology optimization for high-resolution manufacturable microstructures. Int J Numer Methods Eng 113(8):1148–1163
- Groen JP, Wu J, Sigmund O (2019) Homogenization-based stiffness optimization and projection of 2D coated structures with orthotropic infill. Computer Methods in Applied Mechanics and Engineering
- Hassani B, Hinton E (1998) A review of homogenization and topology optimization i - homogenization theory for media with periodic structure. Comput Struct 69(6):707–717
- Hashin Z, Shtrikman S (1962) A variational approach to the theory of the elastic behaviour of polycrystals. J Mech Phys Solids 10(4):343–352
- Huang X, Radman A, Xie YM (2011) Topological design of microstructures of cellular materials for maximum bulk or shear modulus. Comput Mater Sci 50(6):1861–1870. arXiv:0702674v1
- Huang X, Zhou SW, Xie YM, Li Q (2013) Topology optimization of microstructures of cellular materials and composites for macrostructures. Comput Mater Sci 67:397–407
- Jog CS, Haber RB, Bendsøe MP (1994) Topology design with optimized, self-adaptive materials. Int J Numer Meth Eng 37(8):1323–1350
- Kočvara M, Stingl M, Zowe J (2008) Free material optimization: recent progress. Optimization 57(1):79–100
- Li H, Luo Z, Gao L, Qin Q (2018) Topology optimization for concurrent design of structures with multi-patch microstructures by level sets. Comput Methods Appl Mech Eng 328:340–364
- Liu ST, Cheng GD, Gu Y, Zheng XG (2002) Mapping method for sensitivity analysis of composite material property. Struct Multidiscip Optim 24(3):212–217

- Liu L, Yan J, Cheng G (2008) Optimum structure with homogeneous optimum truss-like material. Comput Struct 86(13-14):1417–1425
- Liu C, Du Z, Zhang W, Zhu Y, Guo X (2017) Additive manufacturingoriented design of graded lattice structures through explicit topology optimization. J Appl Mech 84(8):081008
- Liu K, Detwiler D, Tovar A (2018a) Cluster-based optimization of cellular materials and structures for crashworthiness. J Mech Des 140(11):111412
- Liu J, Gaynor AT, Chen S, Kang Z, Suresh K, Takezawa A, Li L, Kato J, Tang J, Wang CC, Cheng L, Liang X, To AC (2018b) Current and future trends in topology optimization for additive manufacturing. Struct Multidiscip Opt 57(6):2457–2483
- Lloyd SP (1982) Least squares quantization in PCM. IEEE Trans Inf Theory 28(2):129–137
- Milton GW, Cherkaev AV (1995) Which elasticity tensors are realizable? J Eng Mater Technol 117(4):483
- Nakshatrala PB, Tortorelli DA, Nakshatrala KB (2013) Nonlinear structural design using multiscale topology optimization. Part I: Static formulation. Comput Meth Appl Mech Eng 261-262:167–176
- Novotny AA, Feijóo RA, Taroco E, Padra C (2003) Topological sensitivity analysis. Comput Methods Appl Mech Eng 192(7-8):803–829
- Osanov M, Guest JK (2016) Topology optimization for architected materials design. Annu Rev Mater Res 46(1):211–233
- Pantz O, Trabelsi K (2008) A post-treatment of the homogenization method for shape optimization. SIAM J Control Optim 47(3):1380–1398
- Pedersen P (1989) On optimal orientation of orthotropic materials. Structural Optimization 1(2):101–106
- Rodrigues HC, Guedes JM (2002) Hierarchical optimization of material and structure. Struct Multidiscip Opt 24(1):1–10
- Schury F, Stingl M, Wein F (2012) Efficient two-scale optimization of manufacturable graded structures. SIAM J Sci Comput 34(6):B711–B733. arXiv:1309.5548v1
- Sethian JA, Wiegmann A (2000) Structural boundary design via level set and immersed interface methods. J Comput Phys 163(2):489– 528. arXiv:1011.1669v3
- Sigmund O (1994) Materials with prescribed constitutive parameters: an inverse homogenization problem. Int J Solids Struct 31(17):2313–2329
- Sigmund O (2000) New class of extremal composites. J Mech Phys Solids 48(2):397–428
- Sigmund O (2001) A 99 line topology optimization code written in matlab. Struct Multidiscip Optim 21(2):120–127
- Sigmund O (2007) Morphology-based black and white filters for topology optimization. Struct Multidiscip Optim 33(4-5):401–424
- Sigmund O, Maute K (2013) Topology optimization approaches: a comparative review. Struct Multidiscip Optim 48(6):1031–1055
- Sigmund O, Torquato S (1997) Design of materials with extreme thermal expansion using a three-phase topology optimization method. J Mech Phys Solids 45(6):1037–1067
- Sigmund O, Aage N, Andreassen E (2016) On the (non-)optimality of Michell structures. Struct Multidiscip Optim 54(2):361–373
- Sivapuram R, Dunning PD, Kim HA (2016) Simultaneous material and structural optimization by multiscale topology optimization. Struct Multidiscip Optim 54(5):1267–1281
- Vigdergauz SB (1989) Regular structures with extremal elastic properties. Mechanics of Solids 24(3):57–63
- Vigdergauz S (1994) Two-dimensional grained composites of extreme rigidity. J Appl Mech 61(2):390
- Vogiatzis P, Chen S, Wang X, Li T, Wang L (2017) Topology optimization of multi-material negative poisson's ratio metamaterials using a reconciled level set method. CAD Computer Aided Design 83:15–32
- Wang M, Wang X, Guo D (2003) A level set method for structural topology optimization. Comput Methods Appl Mech Eng 192(1-2):227–246

- Wang Y, Chen F, Wang MY (2017a) Concurrent design with connectable graded microstructures. Comput Methods Appl Mech Eng 317:84–101
- Wang Y, Xu H, Pasini D (2017b) Multiscale isogeometric topology optimization for lattice materials. Comput Methods Appl Mech Eng 316:568–585
- Xie YM, Steven GP (1993) A simple evolutionary procedure for structural optimization. Comput Struct 49(5):885–896
- Xie YM, Yang X, Shen J, Yan X, Ghaedizadeh A, Rong J, Huang X, Zhou S (2014) Designing orthotropic materials for negative or zero compressibility. Int J Solids Struct 51(23-24):4038–4051
- Xu L, Cheng G (2018) Two-scale concurrent topology optimization with multiple micro materials based on principal stress orientation. Struct Multidiscip Optim 57(5):2093–2107
- Yan X, Huang X, Zha Y, Xie YM (2014) Concurrent topology optimization of structures and their composite microstructures. Comput Struct 133:103–110

- Yang XY, Xei YM, Steven GP, Querin OM (1999) Bidirectional evolutionary method for stiffness optimization. AIAA J 37(11):1483–1488
- Zhang W, Sun S (2006) Scale-related topology optimization of cellular materials and structures. Int J Numer Methods Eng 68(9):993–1011
- Zhang Y, Xiao M, Li H, Gao L, Chu S (2018) Multiscale concurrent topology optimization for cellular structures with multiple microstructures based on ordered SIMP interpolation. Comput Mater Sci 155:74–91
- Zhou S, Li Q (2008) Design of graded two-phase microstructures for tailored elasticity gradients. J Mater Sci 43(15):5157–5167
- Zhu Y, Li S, Du Z, Liu C, Guo X, Zhang W (2019) A novel asymptoticanalysis-based homogenisation approach towards fast design of infill graded microstructures. J Mech Phys Solids 124:612–633

Publisher's note Springer Nature remains neutral with regard to jurisdictional claims in published maps and institutional affiliations.

